Check for updates

RESEARCH ARTICLE

Preliminary characterisation of titanium nitride kinetic inductance travelling-wave parametric amplifiers

[version 1; peer review: 1 approved with reservations, 1 not approved]

Joseph Longden[1], Christine Chaumont[2], Nikita Klimovich[1], Samuel Wood[1], Faouzi Boussaha[2], Boon-Kok Tan[1]

[1]Department of Physics (Astrophysics), University of Oxford, Oxford, OX1 3RH, UK
[2]GEPI (CNRS UMR 8111), Observatoire de Paris, Paris, Île-de-France, France

v1 **First published:** 17 Apr 2025, **5**:109
https://doi.org/10.12688/openreseurope.19884.1
Latest published: 17 Apr 2025, **5**:109
https://doi.org/10.12688/openreseurope.19884.1

Abstract

Background

Kinetic inductance travelling-wave parametric amplifiers (KITWPAs) have proven effective in achieving high gain over broad bandwidths whilst achieving near quantum-limited noise performance, properties which are extremely important for many ultra-sensitive experiments such as radio/millimetre/sub-millimetre astronomy, neutrino mass experiments, and axion dark matter searches, as well as commercial applications like quantum computational and communication systems.

Methods

This paper introduces the preliminary experimental exploration of an alternative KITWPA utilising thin titanium nitride (TiN) films as opposed to the conventionally used niobium titanium nitride (NbTiN) films. TiN films exhibit properties that could be advantageous for KITWPA operation, owing to its controllable critical temperature (T_c) and physical robustness, hence KITWPAs fabricated from TiN films have the potential to replace NbTiN-based TWPAs for various applications, such as reducing the high pump power required to drive a NbTiN TWPA. Our TiN-based KITWPA devices were designed and fabricated with a 42 cm long coplanar waveguide transmission line patterned into a 100 nm thick TiN film, wound in a double spiral fashion to fit into a 2.2×2.2 cm chip.

Results

Open Peer Review

Approval Status ✗ ?

	1	2
version 1 17 Apr 2025	✗ view	? view

1. **Logan Howe**, NIST; University of Colorado, Boulder), Boulder, USA

2. **Luca Fasolo**, "INRiM National Metrology Institute of Italy", Torino, Italy
Andrea Celotto, Polytechnic of Turin Department of Applied Science and Technology, Turin, Italy

Any reports and responses or comments on the article can be found at the end of the article.

We successfully achieved broadband performance, with the best device displaying a peak averaged gain of ~5 dB with a bandwidth of ~3–13 GHz, making this one of the first broadband gain measurements of a TiN KITWPA reported in the literature. Despite this, the measured gain in all batches was lower than simulated due unexpected additional loss mechanisms.

Conclusions

The preliminary results presented here suggest that TiN films are suitable for KITWPA operation, although further investigation is required to improve the gain performance.

Plain language summary

A Kinetic Inductance Travelling-Wave Parametric Amplifier (KITWPA) is a type of device capable of achieving high gain across a broad bandwidth while maintaining the lowest possible noise performance in accordance with the fundamental limits set by nature. These amplifiers play a crucial role in many scientific applications, particularly in cases where the incoming signal is exceptionally weak, such as in astronomy, dark matter searches, quantum computation, and beyond. This article presents the preliminary experimental characterisation of KITWPA devices constructed from titanium nitride (TiN) thin films. We show that our TiN films exhibit several essential properties required for parametric amplifier operation, such as wave mixing, while having the advantage of a controllable gap frequency limit, which is not available to many other superconducting materials, and the ability to lower the required pump power. Our study demonstrates that TiN-based KITWPA devices can also achieve gain over a broad frequency range. The measured peak gain is not as high as expected, primarily due to unexpected losses in the transmission line, likely caused by film's uniformity issues. Nevertheless, this exploration highlights the potential of TiN films for forming broadband travelling-wave amplifiers.

Keywords
Superconducting Parametric Amplifier, Travelling-Wave, Kinetic Inductance, Superconducting Thin Films, Titanium Nitride, High-gap material

This article is included in the European Research Council (ERC) gateway.

This article is included in the Horizon 2020 gateway.

Corresponding authors: Joseph Longden (josephlongden@dualityqp.com), Boon-Kok Tan (boonkok.tan@physics.ox.ac.uk)

Author roles: Longden J: Conceptualization, Data Curation, Formal Analysis, Investigation, Methodology, Software, Validation, Visualization, Writing – Original Draft Preparation, Writing – Review & Editing; **Chaumont C**: Data Curation, Investigation, Resources; **Klimovich N**: Data Curation, Investigation, Methodology, Supervision, Validation, Writing – Review & Editing; **Wood S**: Data Curation, Investigation, Software; **Boussaha F**: Data Curation, Investigation, Resources, Supervision; **Tan BK**: Conceptualization, Funding Acquisition, Investigation, Methodology, Project Administration, Supervision, Validation, Writing – Review & Editing

Competing interests: No competing interests were disclosed.

Grant information: This research was funded by the European Research Council (ERC) under the European Union's Horizon 2020 research and innovation programme with grant agreement No. [803862] (Project [SPA4AstroQIT]). For the purpose of Open Access, the author has applied a CC BY public copyright licence to any Author Accepted Manuscript ver- sion arising from this submission. JC Longden's PhD stu- dentship is fully supported by the UK Science and Tech- nology Facilities Council.
The funders had no role in study design, data collection and analysis, decision to publish, or preparation of the manuscript.

Copyright: © 2025 Longden J *et al*. This is an open access article distributed under the terms of the Creative Commons Attribution License, which permits unrestricted use, distribution, and reproduction in any medium, provided the original work is properly cited.

How to cite this article: Longden J, Chaumont C, Klimovich N *et al.* **Preliminary characterisation of titanium nitride kinetic inductance travelling-wave parametric amplifiers [version 1; peer review: 1 approved with reservations, 1 not approved]** Open Research Europe 2025, **5**:109 https://doi.org/10.12688/openreseurope.19884.1

First published: 17 Apr 2025, **5**:109 https://doi.org/10.12688/openreseurope.19884.1

Introduction

Broadband amplifiers with quantum-limited noise performance and low power consumption are crucial for applications involving ultra-sensitive cryogenic detection systems such as astronomical receivers[1–3], axion dark matter search experiments[4–6], and quantum computation[7–9]. Kinetic inductance travelling-wave parametric amplifiers (KITWPAs)[10–14] are quantum devices, which can achieve high gain over broad bandwidth by efficiently transferring power from a strong 'pump' wave to a weak 'signal' wave via the wave mixing mechanisms in a non-linear medium comprising a high kinetic inductance wire. They are typically realised as long superconducting transmission lines, which are fabricated using films with high normal-state resistivity. They have been experimentally verified to exhibit near quantum-limited noise performance[15] with negligible heat dissipation, whilst their ease of fabrication compared to the Josephson junction based TWPA makes them readily scalable to arrays for large pixel count applications e.g., readout of large astronomical detector arrays and practical large scale quantum computation platforms.

The vast majority of KITWPAs reported in the literature are fabricated using niobium titanium nitride (NbTiN) films, however, in principle, a KITWPA can be fabricated from any superconducting film provided that it possesses the necessary high kinetic inductance and low loss characteristics[16]. In this paper, we experimentally characterise the performance of KITWPAs fabricated from titanium nitride (TiN) films. TiN films have found applications in superconducting micro-resonator detectors e.g., microwave kinetic inductance detectors (MKIDs)[17], due to their high kinetic inductance, controllable critical temperature (T_c) and physical robustness[18]. They have additionally been shown to display low-loss behaviour comparable to other superconducting films[19]. Despite this, NbTiN films remains a popular choice for KITWPA fabrication due to their high T_c, making them better suited for applications at higher bath temperatures and higher frequency ranges, such as the readout or pre-amplification of millimetre (mm) heterodyne receivers.

A plethora of microwave applications at sub-Kelvin temperatures remain, however, such as the readout of astronomical bolometric receivers and first-stage sensors for axion search experiments, and in some of these cases, the high pump power required for driving a NbTiN-KITWPA may affect the overall system sensitivity. We, therefore, intend to explore the use of lower T_c TiN films for such applications and investigate whether there are additional advantages and/or limitations compared to the more conventional NbTiN films. Of particular interest, is whether such TiN KITWPA technology holds the potential to be directly integrated with front-end detectors fabricated with the same material, such as an array of TiN-based MKIDs[17].

Methods

Previous investigations[20,21] have demonstrated that TiN films display the necessary non-linear behaviour required for wave mixing and, hence, potentially parametric amplification. In this paper, therefore, we proceed with the design and characterisation of full KITWPA devices. Figure 1(a) shows a Computer Aided Design (CAD) image of our TiN-KITWPA, which has been designed using the methodology presented in 16. The device comprises a 42 cm long coplanar waveguide (CPW) transmission line containing 300 unit cells patterned onto a 22 mm by 22 mm chip. Figure 1(b) shows a zoom-in of a section of the CAD image, highlighting the spacing of 175 μm between adjacent lines, and the periodic loading structure. The 100 nm thin TiN transmission line coupled with capacitive stubs (or fingers) has a nominal characteristic impedance of 50 Ω with perturbations to the impedance made every 460 μm with lengths of 48 μm. Most of the perturbations have a characteristic impedance of 60 Ω to create a large band gap near 20 GHz and integer multiples thereof. Every third loading has a characteristic impedance of 70 Ω to create a sub-band-gaps near 6.66 GHz and integer multiples thereof. Figure 1(c) shows a zoom-in of one of the 50 Ω sections of the transmission line, which has a centre-strip width of 2 μm, a gap width of 2 μm, and a finger length of 71 μm. The device dimensions are summarised in Table 1.

The TiN-KITWPA devices were fabricated in the clean-room facilities at the Observatoire de Paris using standard sputter deposition, photolithography, and lift-off techniques, which have previously been described in 17,22. The TiN films are reactively sputtered onto a 2-inch diameter substrate made from either high resistivity (>15 kΩ cm), <100>-oriented silicon or 99.999% high-purity, c-plane mono-crystalline sapphire, each with a thickness of 500 μm. Typically, the deposition of the film is done using a 99.995% titanium target with a nitrogen (N_2) flow rate of 5.2 sccm and an argon (Ar) flow rate of 50 sccm at a total pressure of 0.6 Pa with 700 W DC power. Nevertheless, the flexibility to tune the sputtering process parameters allows us to optimise and fine-tune the desired properties of the film. The films produced for our KITWPA devices have target parameters of ρ_N = 140 μΩ cm, T_c = 4.39 K, and a film thickness of t = 100 nm.

Figure 1(d) shows the simulated S_{21} transmission profile, highlighting the first three band gaps, which are created by the periodic impedance perturbation sections described earlier. Figure 1(e) shows the simulated gain-bandwidth profile for different pump current (I_p) values for f_p = 6.41 GHz, and Figure 1(f) shows the gain as a function of input signal current for different I_p values for f_p = 6.41 GHz and f_s = 5 GHz. The gain performance of the KITWPA design has been calculated by numerically solving the coupled-mode equations (CMEs) in a degenerated pump four wave mixing regime, as described in 16.

Experimental setup

The fabricated KITWPA samples are mounted in a gold-plated copper sample holder and are wire bonded to a copper-clad grounded CPW line etched into a 0.51 mm thick Rogers Duroid® RO4350B printed circuit board (PCB), which is connected to the required SubMiniature version A (SMA) interfaces for connection to the external circuitry. The sample

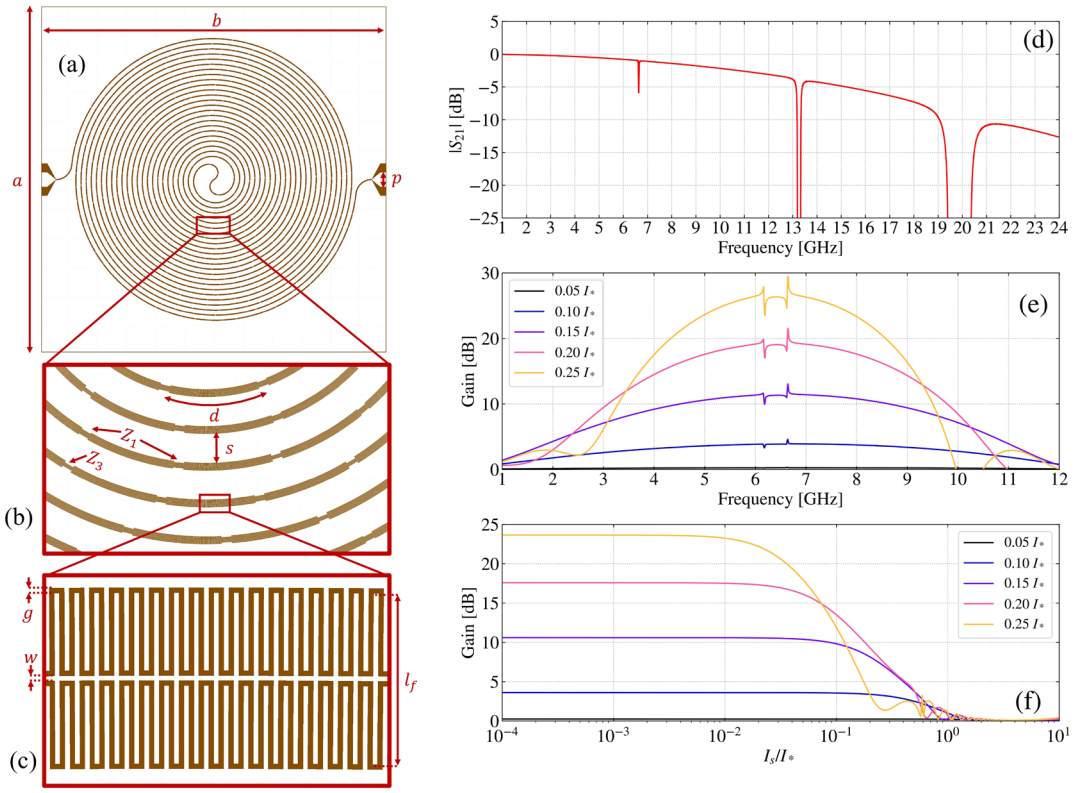

Figure 1. Design layout of the 100 nm TiN KITWPA chip. (**a**) CAD image of the full KITWPA device, including bonding pads. (**b**) Zoom-in of double-spiral winding structure, highlighting the spacing between the spiral arms and the positions of the periodic loadings. (**c**) Zoom-in of the 50 Ω section, highlighting the fishbone structure of the transmission line. The brown regions indicate the areas where the TiN film has been etched away. (**d**) Simulated transmission profile of the device. (**e**) Examples of simulated gain profiles at different pump powers. (**f**) Compression points predicted for the device at different pump powers. Full chip details reported in 23.

Table 1. Physical dimensions of the TiN CPW KITWPA devices described in this paper.

Parameter	Symbol	Unit	Value
Chip Width	a	mm	22
Chip Length	b	mm	22
Bond Pad Width	p	μm	960
Periodic Loading Separation	d	μm	460
Spiral Arm Separation	s	μm	175
Main Line Impedance	Z_0	Ω	50
Primary Loading Impedance	Z_1	Ω	60
Third Loading Impedance	Z_3	Ω	70
Centre-Strip Width	w	μm	2
CPW Gap Width	g	μm	2
Finger Length	l_f	μm	71

holders are then mounted to the mixing stage of a Bluefors® LD250 dilution refrigerator (DR), which cools the devices down to ~10 mK.

Figure 2 shows a schematic of the cryogenic experimental setup used to characterise the KITWPA devices. The setup comprises an Anritsu® Vector-Star MS4644B vector network analyser (VNA) used to provide a swept-frequency signal tone. The pump tone is provided by an Anritsu® Rubidium MG36241A signal generator (SG), which is coupled to the signal tone via a room temperature RF-Lambda® RFDC5M18G10 directional coupler. After warm attenuation, the combined signal/pump tones are injected into the DUT (device-under-test) anchored at the 10 mK stage of the DR. The output signal from the DUT is then routed back to the VNA via a series of low-loss radio frequency (RF) coaxial lines. A DC current can also be provided by a Keithley® 6221 programmable current source and injected along the length of the transmission line using a pair of Sematron® 8810SMF2-26 cryogenic bias tees to operate the DUT in the 3WM operation mode. Additionally, a pair of Radiall® R591762600 6-way

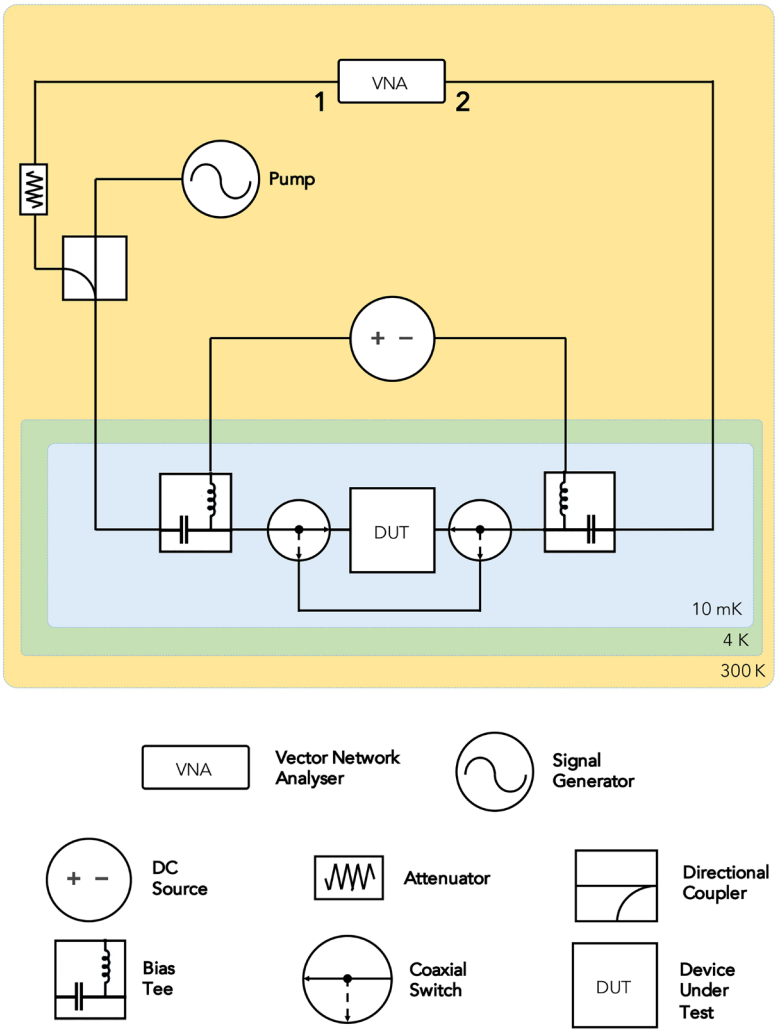

Figure 2. Schematic of cryogenic experimental setup used to characterise the KITWPA devices.

actuator-operated coaxial switches at the cryogenic stage are utilised to switch between multiple DUTs and a through line, to allow for in-situ cryogenic calibration. A Keithley® 2182A nanovoltmeter is used to measure the voltage across the KITWPA devices, when needed.

Results

Summary of the fabricated batches

We have fabricated seven different batches of TiN KITWPA devices in total, with each batch containing five KITWPA devices. The key properties of each batch are summarised in Table 2.

Unfortunately, the first two batches did not result in any useful devices, as the long transmission lines were either open- (see example in Figure 3(a)) or short-circuited (see Figure 3(b)). A detailed examination of the fabrication process found that the wavelength of the UV light used in the photo-lithography process (365 nm) was too long, leading to poorly-defined line edges. For long and narrow transmission line structures, such as the devices presented here, a shorter wavelength of 320 nm is more appropriate. The adoption of this shorter wavelength for subsequent batches led to a fabrication yield of 20–40%, which whilst still low, is sufficient to characterise the KITWPA devices.

The KITWPA shown in Figure 1 was designed and simulated using an assumed film resistivity of ρ_N = 140 μΩ cm, however, subsequent measurements of the film resistivity of each batch using a four-point probe revealed a considerable variation in ρ_N between each batch. This variation is shown in Table 2, highlighting how ρ_N for batches 3 and 4 deviates from the design value by a factor of over 2.5. Whilst the reason for this resistivity variation is not completely clear at the moment, one possible reason could be due to erosion of the Ti target used in the sputtering process, which could lead to

Table 2. Summary of the fabricated TiN CPW KITWPA batches, where $\rho_{N,Measured}$ is the measured normal-state resistivity of the film, $t_{Measured}$ is the measured thickness of the film, $Z_{Recalculated}$ is the recalculated characteristic impedance of the transmission line, and n_{loss} is the surface resistance correction factor.

Batch	Substrate	$\rho_{N,Measured}$ (μΩ cm)	No. Surviving (/5)	$t_{Measured}$ (nm)	$Z_{Recalculated}$ (Ω)	n_{loss} (%)
1	Sapphire	-	0	97	-	-
2	Sapphire	-	0	97	-	-
3	Sapphire	380	1	96	85	5
4	Sapphire	380	2	106	81	5
5	Sapphire	200	2	106	63	10
6a	Sapphire	120	1	95	55	50
6b	Silicon	120	1	95	51	40

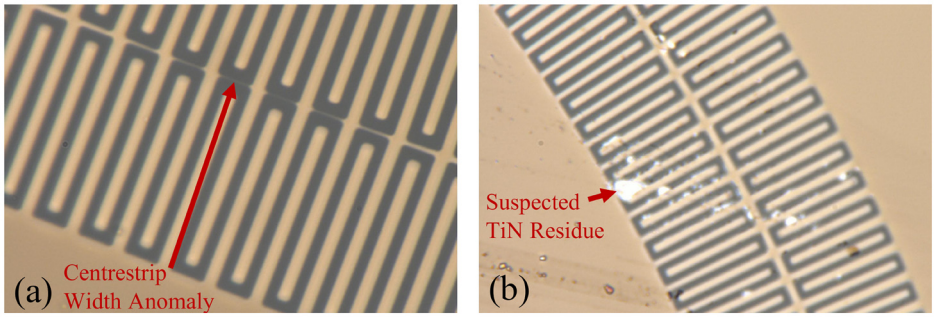

Figure 3. (**a**) Possible hotspot/open-circuit in transmission line. (**b**) Possible short-circuit in transmission line, with the white debris likely to be residual TiN not successfully etched away. Gold coloured areas highlight the regions were the TiN film is deposited.

drifts in the fabrication parameters used when sputtering TiN films[24]. In subsequent batches, we managed to achieve ρ_N values closer to the design value by reducing the pressure in the sputtering machine from 0.6 Pa to 0.4 Pa. The first five batches were fabricated using sapphire substrates, however, to investigate the effect that the substrate material may have on the performance of the TiN KITWPA, we additionally fabricated a batch on silicon during our sixth fabrication run, where batch 6a denotes a sapphire substrate and 6b denotes a silicon substrate.

Figure 4 shows the un-pumped transmission spectrum for a single device from each batch (except batch 2), where the raw data is shown in light grey and the smoothed (averaged every 100 data points) data is shown in orange. The transmission spectrum for the batch 1 chip is included to show the transmission of a device with defects such as those highlighted in Figure 3. For the devices that are not short- or open-circuited, we see that the 'envelope' of the transmission spectra are closer to 0 dB, plus we also observe the presence of periodic band gaps. The positions of the band gaps, however, are different to those simulated in Figure 1(d), which can be explained by the deviation in ρ_N and film thickness from the simulated parameters. This variation additionally means that the characteristic impedance of each transmission line would have deviated from the 50 Ω design value, causing an impedance mismatch at the two ends of the KITWPA. This is evident from the ripples in the raw transmission spectra in Figure 4, which are largest for batches 3 and 4 since they have the largest deviation in measured resistivity from Table 2, hence the largest mismatch to 50 Ω.

For batches 3–6b, we re-simulated the transmission spectra using the measured ρ_N and thickness parameters given in Table 2, with the assumed gap voltage, V_{gap} = 1.33 mV. The results are denoted by the dashed black curves in Figure 4, which show that for each batch, the frequency of the simulated first band gap is still approximately 1 GHz higher. Another feature to note from these re-simulations is the difference between the simulated and measured 'envelope' of the spectrum. For batches 3 and 4, which have the highest resistivity, the measured transmission is much higher than the simulation performed using the

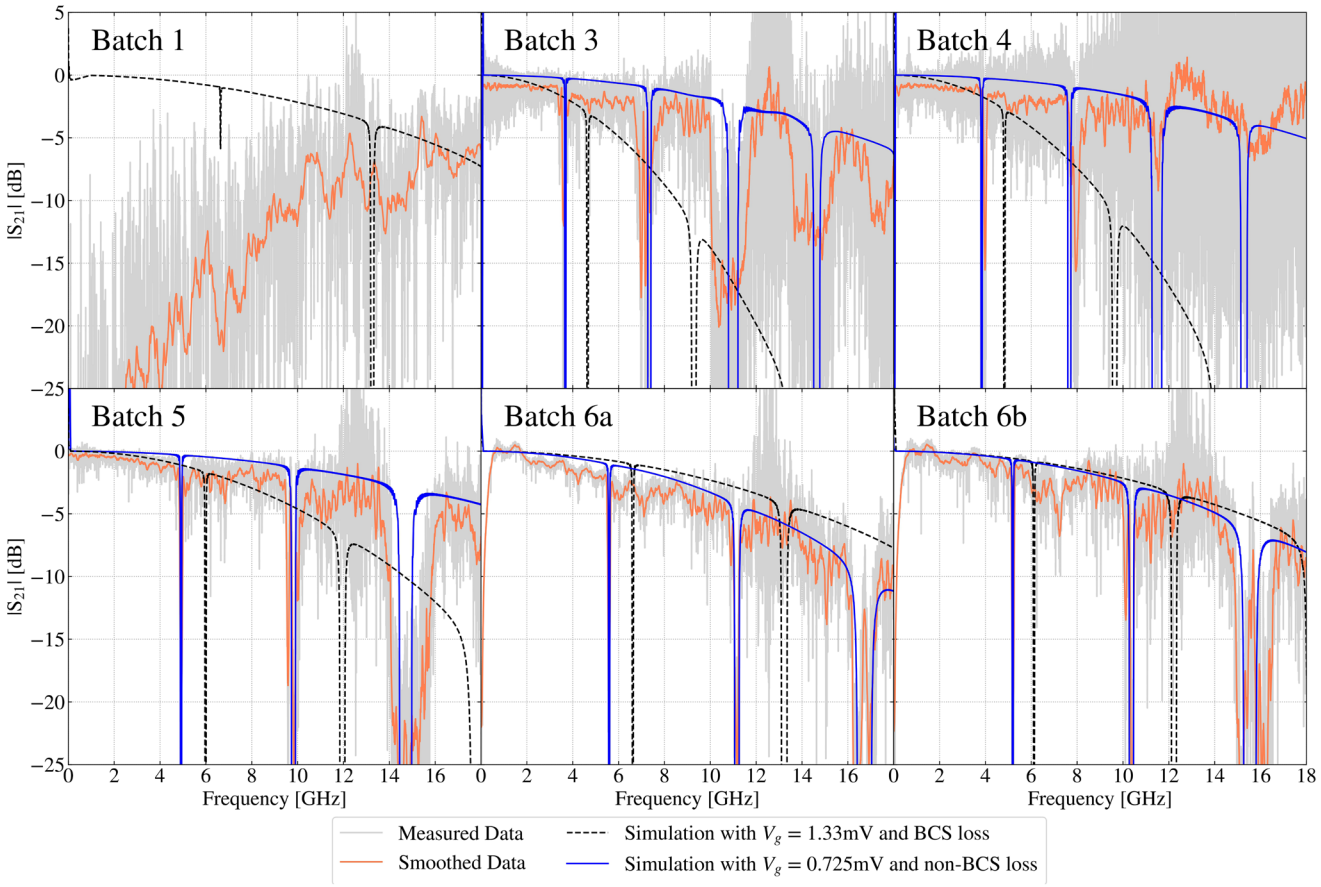

Figure 4. Un-pumped transmission profile of KITWPA devices from different fabrication batches as summarised in Table 2. The simulated transmission curves for each batch were calculated using the methodology in 16. For Batch 5, 6a & 6b, the measured first band gap may not be clearly visible as it coincides exactly with the simulated curve.

standard BCS (Bardeen-Cooper-Schieffer) theory. This implies that the film is much less lossy than expected for a BCS film, suggesting it would be suitable for use as KITWPA. For the batches with a lower film resistivity, however, we see that this discrepancy is less significant, especially for batch 6b. We can quantify this behaviour by introducing a constant, n_{loss}, defined by,

$$n_{loss} \equiv R_s^{(Measured)} / R_s^{(BCS)} \quad (1)$$

where $R_s^{(Measured)}$ is the measured surface resistance of the film and $R_s^{(BCS)}$ is the surface resistance of the film calculated from standard BCS theory. Using this n_{loss} parameter, as well as allowing V_{gap} to be a free-fitting parameter to recover the true value of both parameters, we further re-simulate our transmission spectra. These results are illustrated by the blue curves in Figure 4, where for each batch we reduced the simulated gap voltage of the film to V_{gap} = 0.725 mV instead of the expected V_{gap} = 1.33 mV. The positions of simulated band gaps now match very well to the measured ones, which suggests that V_{gap} of our TiN films is much lower than expected, although the reason for this is not completely clear. One possible explanation could be a systematic error in our fabrication process[16], as the V_{gap} of our TiN film is sensitive to the nitrogen flow rate in the sputtering machine. Another possibility is that this behaviour is due to some microphysical behaviour that we have not taken into account, such as the smearing of the superconducting gap[25–27].

The n_{loss} values used for each re-simulation are summarised in Table 2, and from this we see a clear ρ_N-dependence on the value of n_{loss}, with the films with higher ρ_N resulting in a lower n_{loss}. For all batches, we notice that $n_{loss} < 100\%$ i.e., the films appear to be less lossy than expected from BCS theory, which is a desired feature for TWPA operation. It should be noted that n_{loss} is not a fundamental parameter, but simply a free parameter we use to recover the true value of R_s. Nevertheless, this clear dependence of n_{loss} on ρ_N is an indication that some microphysics beyond standard BCS theory is required to better understand the behaviour of our TiN films.

Device characterisations

The non-linear kinetic inductance for a superconducting transmission line exhibits a quadratic current-dependence in the limit of small currents,

$$L_k(I) = L_{k0}(1 + (I / I_*)^2). \quad (2)$$

The I_* term can be obtained from measuring the change in the phase of S_{21} in response to an applied current by equating the two expressions for the phase velocity of a transmission line,

$$v_{ph} = 1/\mathrm{sqrt}(LC) = \omega / k, \quad (3)$$

to produce a relationship between the fractional change in the wavevector, k, and the fractional change in L i.e.,

$$L_k(I)/L_{k0} = (k(I)/k(I=0))^2. \quad (4)$$

A stronger phase shift would be observed for a stronger applied DC current, hence we can plot the fractional change in L_k against the applied DC current. Fitting the data with the quadratic expression for the current-dependent kinetic inductance allows the value of I_* to be recovered, as shown in Figure 5 for one of the devices from batch 6b, resulting in I_* = 11.29 mA for this particular device.

To probe other non-linear properties of the TiN film, we make use of some test structure devices (short transmission line coupled with lumped-element TiN resonators[21]) such as those shown in Figure 6(a). Figure 6(b) shows the $|S_{21}|$ of the resonator as the input power from the VNA is increased, and from this we see that for powers up to –20 dBm, the resonator shifts to lower frequencies without the depth in the resonance changing, suggesting that the film is operating in a lossless non-linear regime. For higher powers beyond this maximum lossless power point $P_{lossless}$, the depth of the resonance starts to decrease, suggesting the film has now entered a lossy non-linear regime.

Figure 7(a)–(b) show the change in the transmission spectrum for the batch 4 and batch 6b devices, respectively, when pumped just below the first band gap at a power level of 1 dB below the critical current. Instead of amplifying, as one would expect when pumped, the transmission through the devices decreases, with the magnitude of the losses in each chip being broadly identical when normalised by the pump frequency, f_p, to take into account the difference in the effective electrical lengths between the two chips due to the different resistivities. On initial inspection, this pump-induced loss appears unexpected, however, when comparing the pump powers used in Figure 7 with the RF powers applied to the resonators in Figure 6(b), we see that the pump powers in the KITWPA devices are much higher than $P_{lossless}$, implying that our KITWPA devices are in fact operating in a lossy regime now. This implies that the KITWPA devices may not work properly in their designed DP-4WM regime, as the pump powers required to achieve the simulated gain lead to unexpected losses that would negate any possible gain from wave mixing. Reducing the pump power to be lower than $P_{lossless}$ would result in too weak a pump power to promote sufficient wave mixing in order to achieve the desired gain, hence we would require a much longer transmission line to achieve usable gain.

The mechanisms behind the observed pump-induced losses are not completely clear at the moment. We believe that the two most likely physical mechanisms are unexpected multiple photon Cooper pair breaking, or parasitic wave mixing, whereby unwanted frequency conversion mechanisms are stealing energy away from the signal frequency by converting it to other frequencies. The two loss mechanisms can conveniently be distinguished, however, by using the fact that as with parametric amplification, parasitic wave mixing is only expected to occur when the pump and signal tones are co-propagating along

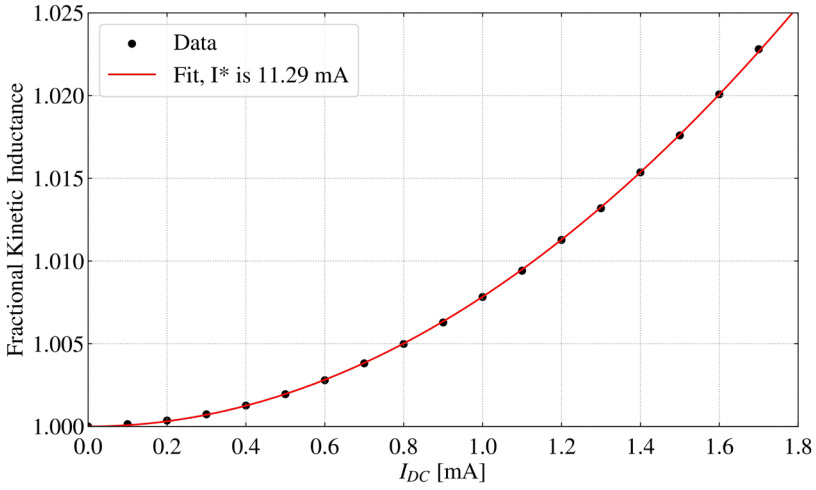

Figure 5. Fractional kinetic inductance as a function of applied DC current for a batch 6b device. The data were fitted with $L = 1 + I_{DC}$ to give an estimated I_* = 11.29 mA.

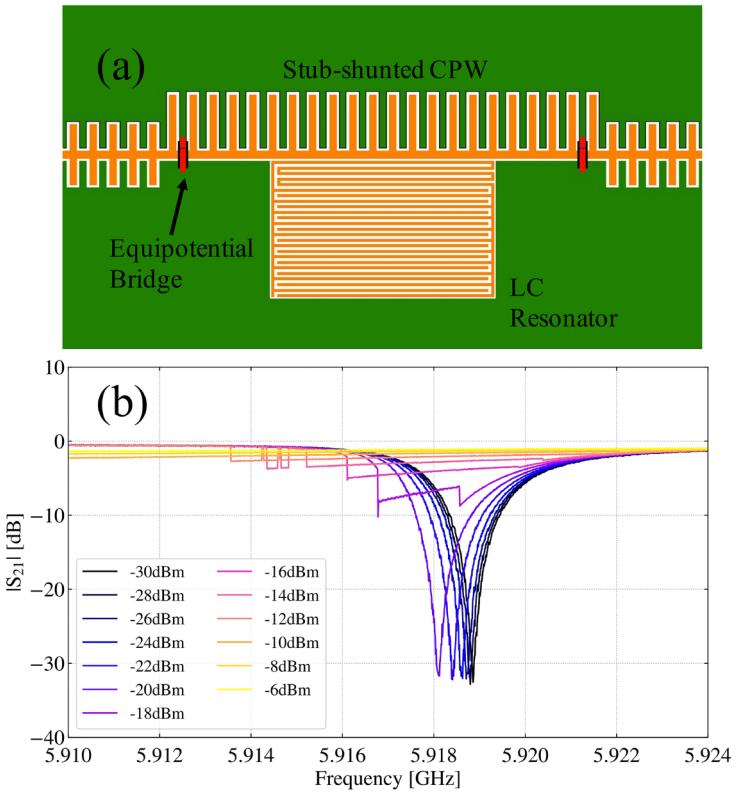

Figure 6. (**a**) CAD image of a lumped element LC resonator shunted to a 50 Ω transmission line. Note that the red equipotential bridges[20] are not included on the fabricated chip. (**b**) Shift in the resonance frequency and depth as the input power from the VNA is increased.

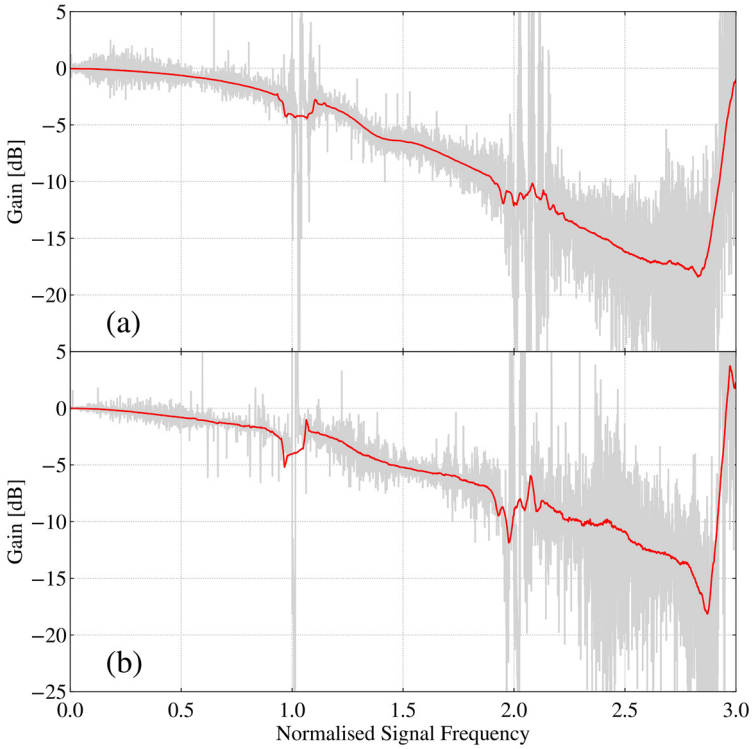

Figure 7. (**a**) Transmission profile for batch 4 device with pump tone at 3.75 GHz and –14.00 dBm. (**b**) Transmission profile for batch 6b device with pump tone at 5.10 GHz and –7.00 dBm. In both plots, the frequency is normalised by the pump frequency, f_p.

the KITWPA in the same direction, as the phase matching conditions for when the pump and signal are anti-propagating are different[28], hence parametric process will be suppressed in this case. Conversely, Cooper pair breaking will occur independently of the pump propagation direction. By measuring and comparing the change in the forward transmission $\Delta|S_{21}|$, where,

$$\Delta|S_{21}| = |S_{21}|^{(\text{Pump On})} - |S_{21}|^{(\text{Pump Off})}, \quad (5)$$

and the change in the reverse transmission $\Delta|S_{12}|$, where,

$$\Delta|S_{12}| = |S_{12}|^{(\text{Pump On})} - |S_{12}|^{(\text{Pump Off})}, \quad (6)$$

it is possible to identify the responsible loss mechanism.

Figure 8 plots $\Delta|S_{21}|$ and $\Delta|S_{12}|$ for different f_p values. For each pump frequency, the pump power was set to just below I_c to ensure the same amount of power was entering the transmission line at each f_p. Studying the spectra across Figure 8, we observe a large range of variation. For f_p = 1 GHz, 2 GHz, and 3 GHz, we see a stark contrast between $\Delta|S_{21}|$ and $\Delta|S_{12}|$, however, as the pump frequency shifts higher, we observe tha $\Delta|S_{21}|$ gets progressively closer to resembling $\Delta|S_{12}|$. This is strongly indicative that the generation of pump harmonics and/or the interaction between these pump harmonics and f_s, could be the primary source of the observed losses at lower pump frequencies. For f_p > 3 GHz, both the forward and reverse transmission curves are virtually identical, suggesting that these parasitic harmonic wave mixing processes have been suppressed, possibly due to poorer phase matching caused by the stronger non-linear dispersion at higher frequencies.

From the $\Delta|S_{12}|$ spectra, we see that applying a pump tone in the opposite direction to the signal tone also results in losses, albeit with different behaviour below f_p = 3 GHz, which indicates the presence of multi-photon Cooper pair breaking, and possibly pump harmonics generation as well. Figure 9 plots $\Delta|S_{12}|$ as a function of $P_p - P_c$, where $P_c = I_c^2 Z$ is the RF power at which superconductivity is broken for an impedance, Z, for various f_s values. This figure shows a clear increase in $\Delta|S_{12}|$ with increased P_p, suggesting the observed losses are pump power dependent, consistent with the multi-photon Cooper pair breaking mechanism theorised earlier.

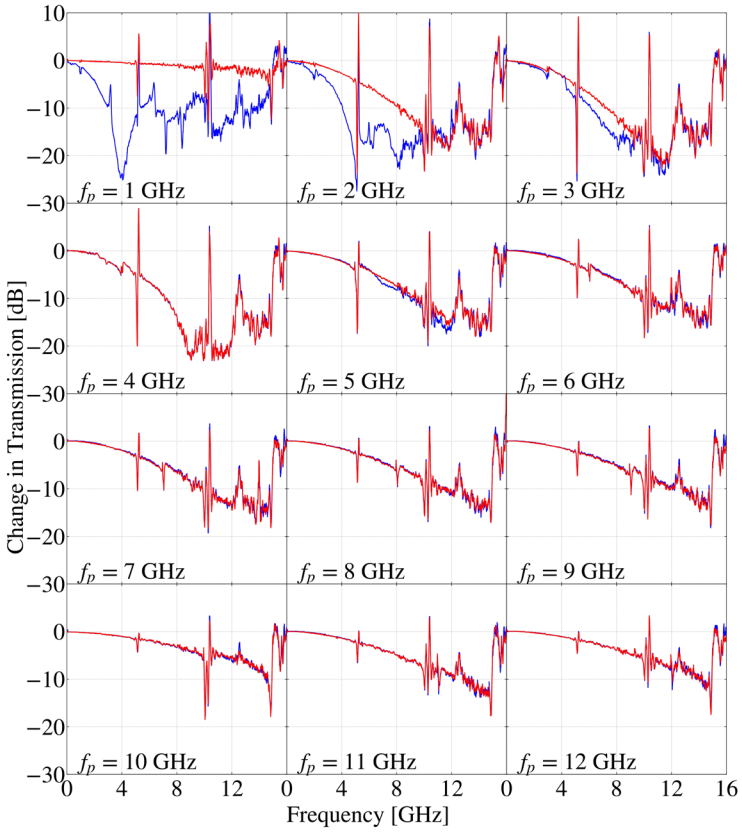

Figure 8. Change in $|S_{21}|$ (blue) and $|S_{12}|$ (red) for different pump frequencies for a batch 6b chip, where for each pump frequency, the power was adjusted to be just below the point at which superconductivity is broken. Note that the sharp peaks near 5 GHz, 10 GHz, and 15 GHz are related to the designated band gaps.

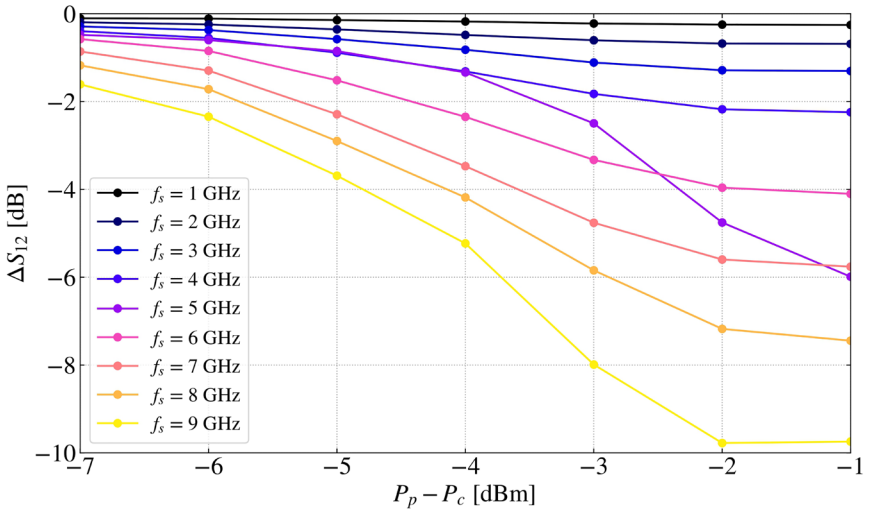

Figure 9. Change in S12 as a function of pump power for different signal frequencies. The pump frequency for each case was 5 GHz. Note that the losses that appear to increase faster at f_s = 5 GHz is due to its proximity to the first band gap, shifting the gap to lower frequencies as the pump power is increased.

DC-3WM measurements

Whilst our TiN film appears to display unexpected multi-photon Cooper pair breaking that significantly affects the gain performance of our KITWPA devices, Figure 8 clearly shows that wave mixing processes are also taking place, as indicated by the difference between $\Delta|S_{21}|$ and $\Delta|S_{12}|$. Since multi-photon Cooper pair breaking requires the presence of RF photons, we could potentially minimise this effect by replacing some of the pump power required to achieve parametric non-linear wave mixing by injecting a DC current instead i.e., operating the device in the DC-3WM regime. Furthermore, we observed in Figure 8 that parasitic harmonic wave mixing processes are suppressed for higher pump frequencies due to poorer phase-matching caused by the stronger non-linear dispersion at higher frequencies. This suggests it would be advantageous to pump the device at higher order stop bands instead of the primary stop band near 5 GHz.

Figure 10(a)–(b) show the gain curves normalised by f_p for a chip from both batch 4 and batch 6b, respectively, operating in the DC-3WM mode when pumped just above the third band gap. Remarkably, both devices exhibit a measurable gain, with the batch 4 device having a peak average gain of approximately 2 dB, and the batch 6b device having a peak average gain of approximately 5 dB.

Aside from the difference in peak average gain, the two plots are noticeably similar in shape, with dips in the gain profiles at roughly 0.3 f_p and 0.6 f_p, which are caused by the presence of the first and second band-gaps in the transmission spectrum, respectively. We additionally notice a pair of dips at roughly 0.4 f_p and 0.7 f_p, which occur when a signal propagating at these frequencies generates an idler, $f_i = f_p - f_s$, that falls into or close to one of the two band-gaps at 0.3 f_p and 0.6 f_p, which suppresses any gain at those frequencies.

As stated previously, it is expected that signal-pump wave mixing only occurs when the pump and signal tones are propagating along the KITWPA in the same direction, meaning that any directionally independent losses can be factored out by measuring the reverse transmission when the pump and DC are applied. Figure 11 plots the forward and reverse 'gain' for the batch 6b chip when DC-biased and pumped above the third stop band. The device behaves as expected, with a clear gain in the forward direction and only a small loss in the reverse direction, which is caused by the Cooper pair breaking mechanism theorised earlier, but weaker due to the higher pump frequency used in this DC-3WM case.

Conclusions

This paper has presented the preliminary characterisation of TiN KITWPA devices. We found that operating the devices in a DC-3WM regime was able to produce a broad-band gain of up to 5 dB over a bandwidth of 9 GHz, however, the measured gain was lower than expected due to unexpected loss mechanisms. The results presented here demonstrate that TiN films display the necessary non-linear behaviour for KITWPA operation but our particular design meant the film was not operating in the desired lossless regime when the pump tone was applied. Measurements of the un-pumped transmission spectra revealed that films with a higher ρ_N displayed much lower losses compared to the BCS simulations, which provides experimental evidence for microphysics beyond standard BCS theory that requires further investigation. These measurements also suggest that higher-ρ_N films are more likely to operate in the desired regime. Comparing to other devices reported

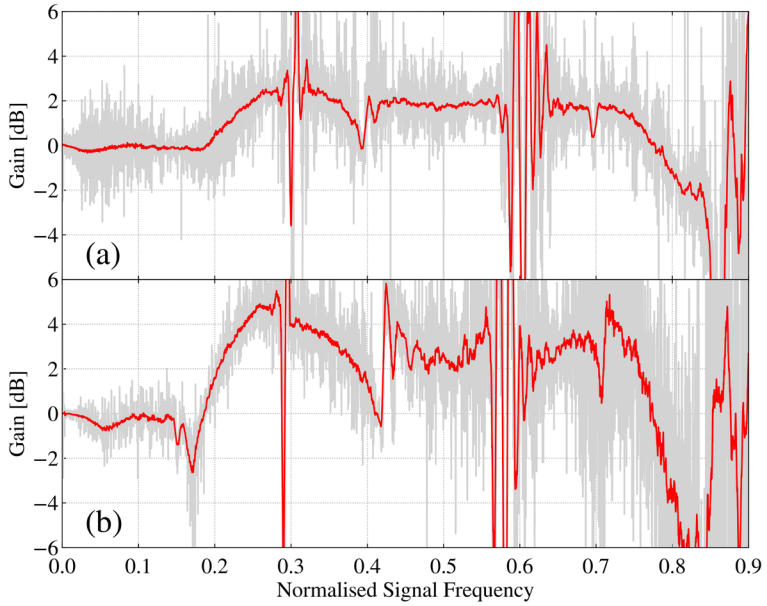

Figure 10. (**a**) DC-3WM gain profile for batch 4 device with f_p = 12.7 GHz, P_p = −21.0 dBm, and I_{DC} = 0.63 mA. (**b**) DC-3WM gain profile for batch 6b device with f_p = 17.7 GHz, P_p = 10.0 dBm, and I_{DC} = 1.53 mA. Each device has been pumped just above the third band gap and in both plots, the frequency is normalised by the pump frequency, f_p.

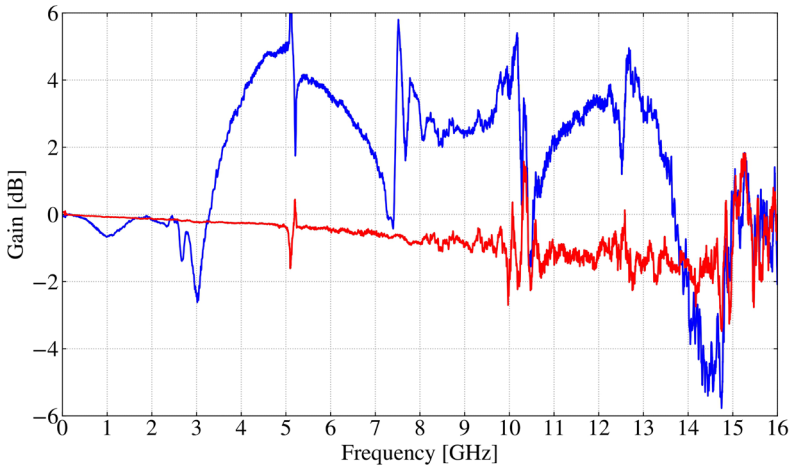

Figure 11. Smoothed DC-3WM gain profile of the batch 6b device when the pump and signal are co-propagating (blue) and when they are anti-propagating (red) when pumped just above the third band-gap.

in the literature, our TiN KITWPAs use thicker films and larger transmission line dimensions. Making modifications to our KITWPA design, therefore, such as using increased ρ_N, decreased thickness, or narrower transmission line width, may further extend the lossless non-linear regime, meaning that TiN could potentially be used as an alternative to NbTiN for the fabrication of high-gain KITWPA devices.

Ethics and consent

Ethical approval and consent were not required.

Data and software availability

Underlying data

Figshare: Preliminary characterisation of titanium nitride kinetic inductance travelling-wave parametric amplifiers https://doi.org/10.6084/m9.figshare.28560917.v1[29]

This project contains the following underlying data, organised by 'dataset' within the Figshare collection:

- Dataset for Figure 4 (Raw datasets in .s2p or .csv for each panel in Figure 4)

- Dataset for Figure 5 (Raw datasets in . s2p for each panel in Figure 5)
- Dataset for Figure 6 (Raw datasets in . s2p for each panel in Figure 6)
- Dataset for Figure 7 (Raw datasets in . s2p for each panel in Figure 7)
- Dataset for Figure 8 (Raw datasets in . s2p for each panel in Figure 8)
- Dataset for Figure 9 (Raw datasets in . s2p for each panel in Figure 9)
- Dataset for Figure 10 (Raw datasets in . s2p for each panel in Figure 10)
- Dataset for Figure 11 (Raw datasets in . s2p for each panel in Figure 11)

Data are available under the terms of the Creative Commons Attribution 4.0 International license (CC-BY 4.0).

Extended data

Figshare: Preliminary characterisation of titanium nitride kinetic inductance travelling-wave parametric amplifiers

https://doi.org/10.6084/m9.figshare.28560932.v1[30]

This project contains the following extended data, organised by 'dataset' within the Figshare collection:

- Plotting script for Figure 4 (Python script in .py that reads & processes the raw data and plots each panel in Figure 4)
- Plotting scripts for Figure 5 (Python script in .py that read & process the raw data and plot each panel in Figure 5)
- Plotting scripts for Figure 6 (Python script in .py that read & process the raw data and plot each panel in Figure 6)
- Plotting script for Figure 7 (Python script in .py that reads & processes the raw data and plots each panel in Figure 7)
- Plotting scripts for Figure 8 (Python script in .py that read & process the raw data and plot each panel in Figure 8)
- Plotting scripts for Figure 9 (Python script in .py that read & process the raw data and plot each panel in Figure 9)
- Plotting script for Figure 10 (Python script in .py that reads & processes the raw data and plots each panel in Figure 10)
- Plotting scripts for Figure 11 (Python script in .py that read & process the raw data and plot each panel in Figure 11)

Data are available under the terms of the Creative Commons Attribution 4.0 International license (CC-BY 4.0).

Acknowledgements

The authors would like to say a special thanks to our group's technician, Rik Elliot, for all his help in building the electronics and mechanical components required for the experiments.

References

1. Noroozian O: **Cycle 5 NRAO ALMA development study report technology development of quantum-limited, ultra-wideband RF amplifiers for ALMA: a 65–150 GHz test case**. 2020.
Reference Source
2. Zobrist N, Eom BH, Day P, *et al.*: **Wide-band parametric amplifier readout and resolution of optical Microwave Kinetic Inductance Detectors.** *Appl Phys Lett.* 2019; **115**(4): 042601.
Publisher Full Text
3. Che G, Gordon S, Day P, *et al.*: **A superconducting phase shifter and Traveling Wave Kinetic Inductance Parametric Amplifier for W-Band astronomy**. 2017.
Publisher Full Text
4. Backes KM, Palken DA, Al Kenany S, *et al.*: **A quantum enhanced search for dark matter axions.** *Nature.* 2021; **590**(7845): 238–242.
PubMed Abstract | **Publisher Full Text**
5. Kutlu Ç, Van Loo AF, Uchaikin SV, *et al.*: **Characterization of a flux-driven Josephson parametric amplifier with near quantum-limited added noise for axion search experiments.** *Supercond Sci Technol.* 2021; **34**(8).
Publisher Full Text
6. Braine T, Cervantes R, Crisosto N, *et al.*: **Extended search for the invisible axion with the axion dark matter experiment.** *Phys Rev Lett.* 2020; **124**(10): 101303.
PubMed Abstract | **Publisher Full Text**
7. Arute F, Arya K, Babbush R, *et al.*: **Quantum supremacy using a programmable superconducting processor.** *Nature.* 2019; **574**(7779): 505–510.
PubMed Abstract | **Publisher Full Text**
8. Lecocq F, Quinlan F, Cicak K, *et al.*: **Control and readout of a superconducting qubit using a photonic link.** *Nature.* 2021; **591**(7851): 575–579.
PubMed Abstract | **Publisher Full Text**
9. Gonzalez-Zalba MF, de Franceschi S, Charbon E, *et al.*: **Scaling silicon-based quantum computing using CMOS technology.** *Nat Electron.* 2021; **4**: 872–884.
Publisher Full Text
10. Eom BH, Day PK, Leduc HG, *et al.*: **A wideband, low-noise superconducting amplifier with high dynamic range.** *Nat Phys.* 2012; **8**(8): 623–627.
Publisher Full Text
11. Bockstiegel C, Gao J, Vissers MR, *et al.*: **Development of a broadband NbTiN traveling wave parametric amplifier for MKID readout.** *J Low Temp Phys.* Springer New York LLC, 2014; **176**: 476–482.
Publisher Full Text
12. Vissers MR, Erickson RP, Ku HS, *et al.*: **Low-noise kinetic inductance traveling-wave amplifier using three-wave mixing.** *Appl Phys Lett.* 2016; **108**(1): 012601.
PubMed Abstract | **Publisher Full Text** | **Free Full Text**
13. Goldstein S, Kirsh N, Svetitsky E, *et al.*: **Four wave-mixing in a microstrip kinetic inductance travelling wave parametric amplifier.** *Appl Phys Lett.* 2020; **116**(15).
Publisher Full Text
14. Shu S, Klimovich N, Eom BH, *et al.*: **Nonlinearity and wide-band parametric**

amplification in a (Nb,Ti)N microstrip transmission line. *Phys Rev Res.* 2021; **3**(2): 1–9.
Publisher Full Text

15. Klimovich N, Day P, Shu S, *et al.*: **Demonstration of a quantum noise limited traveling-wave parametric amplifier**. 2023.
Publisher Full Text

16. Tan BK, Boussaha F, Chaumont C, *et al.*: **Engineering the thin film characteristics for optimal performance of superconducting kinetic inductance amplifiers using a rigorous modelling technique [version 2; peer review: 3 approved].** *Open Res Eur.* 2022; **2**: 88.
PubMed Abstract | **Publisher Full Text** | **Free Full Text**

17. Boussaha F, Beldi S, Monfardini A, *et al.*: **Development of TiN vacuum-gap capacitor lumped-element kinetic inductance detectors.** *J Low Temp Phys.* 2020; **199**(3–4): 994–1003.
Publisher Full Text

18. Leduc HG, Bumble B, Day PK, *et al.*: **Titanium nitride films for ultrasensitive microresonator detectors.** *Appl Phys Lett.* 2010; **97**(10): 1–4.
Publisher Full Text

19. Mazin BA: **Superconducting materials for Microwave Kinetic Inductance Detectors**. 2020.
Publisher Full Text

20. Longden JC, Boussaha FM, Chaumont C, *et al.*: **Preliminary characterisation of titanium nitride thin film at 300 mK for the development of kinetic inductance travelling wave parametric amplifiers.** *Quantum Technology: Driving Commercialisation of an Enabling Science II.* 2021; **1188113**: 38.
Publisher Full Text

21. Longden JC, Boussaha F, Chaumont C, *et al.*: **Measuring the non-linearity of titanium nitride film for applications as kinetic inductance travelling wave parametric amplifiers.** In: *Proceedings of the 32nd International Symposium on Space Terahertz Technology*. 2022.

22. Nicaise P: **Development of Microwave Kinetic Inductance Detectors for applications in optical to near-IR astronomy.** PhD thesis, Observatoire de Paris, PSL Université, 2022.
Reference Source

23. Longden JC: **Development of superconducting thin film travelling wave parametric amplifiers.** Oxford University, 2023.
Reference Source

24. Vissers MR, Gao J, Kline JS, *et al.*: **Characterization and in-situ monitoring of sub-stoichiometric adjustable superconducting critical temperature titanium nitride growth.** *Thin Solid Films.* 2013; **548**: 485–488.
Publisher Full Text

25. Driessen EFC, Coumou PCJJ, Tromp RR, *et al.*: **Strongly disordered TiN and NbTiN *s*-wave superconductors probed by microwave electrodynamics.** *Phys Rev Lett.* 2012; **109**(10): 107003.
PubMed Abstract | **Publisher Full Text**

26. Sacépé B, Chapelier C, Baturina TI, *et al.*: **Disorder-induced inhomogeneities of the superconducting state close to the superconductor-insulator transition.** *Phys Rev Lett.* 2008; **101**(15): 157006.
PubMed Abstract | **Publisher Full Text**

27. Feigel'man MV, Skvortsov MA: **Universal broadening of the Bardeen-Cooper-Schrieffer coherence peak of disordered superconducting films.** *Phys Rev Lett.* 2012; **109**(14): 147002.
PubMed Abstract | **Publisher Full Text**

28. Planat L, Ranadive A, Dassonneville R, *et al.*: **A photonic crystal Josephson traveling wave parametric amplifier.** *Phys Rev X.* 2020; **10**: 021021.
Publisher Full Text

29. Longden J: **Underlying Data.** figshare. Dataset, 2025.
http://www.doi.org/10.6084/m9.figshare.28560917.v1

30. Longden J: **Plotting Scripts**. *figshare*. Software, 2025.
http://www.doi.org/10.6084/m9.figshare.28560932.v1

Open Peer Review

Current Peer Review Status: ✗ ?

Version 1

Reviewer Report 29 May 2025

https://doi.org/10.21956/openreseurope.21510.r53464

© **2025 Fasolo L et al.** This is an open access peer review report distributed under the terms of the Creative Commons Attribution License, which permits unrestricted use, distribution, and reproduction in any medium, provided the original work is properly cited.

?

Luca Fasolo
"INRiM National Metrology Institute of Italy", Torino, Italy
Andrea Celotto
Polytechnic of Turin Department of Applied Science and Technology, Turin, Italy

The manuscript presents a perspective on the use of TiN films for the fabrication of Kinetic Inductance Traveling Wave Parametric Amplifiers. The design and optimization of the fabrication processes are described in detail, and the analysis of the discrepancies between targeted and measured performance is thoroughly discussed. Although no gain was observed in the 4WM regime in these preliminary batches, a modest gain was achieved in the 3WM regime, representing a solid foundation for future iterations in the modelling-design-fabrication cycle.

Our most substantial remarks concern the interpretation of the device behaviour in what the authors describe as a 'lossy' regime, the attribution of pump power-dependent transmission losses solely to quasiparticle generation, and the interpretation of results reported in Figure 8. These and other comments are listed below, following the order of appearance in the manuscript.

Methods

- **In the second paragraph the symbol ρN for the normal-state resistivity is not properly introduced.**
- **We suggest adding in Figure 1(f)'s caption that the curves are referred to a single signal frequency, as correctly reported in the main text.**
- **The authors should properly introduce the quantity "I*" before using it in Figure 1(e) and 1(f). We also suggest adding titles to the figure legends to improve readability.**
- **Since the authors state that the full chip details are reported in [23], they might consider removing Table 1, which presents several but not all the chip's key parameters (for instance, the finger length is provided only for the 50-ohm sections, but not for sections Z1 and Z3). Alternatively, the authors could consider including the missing parameters in the table to make it more complete.**

- **In the last sentence of the final paragraph, we recommend specifying the order of approximation used in the analytical solution via CME, in accordance with the commonly accepted nomenclature reported in (10.1103/PhysRevApplied.14.034058). We assume that the approach adopted corresponds to a CME-1, which neglects all effects related to spurious frequency generation.**

Experimental setup

- **In the first paragraph, the statement 'which cools the devices down to ~10 mK' may be too strong, as it is widely acknowledged that a discrepancy often exists between the mixing chamber plate temperature and the actual chip temperature. We suggest rephrasing it with a more cautious expression, such as '...with a base temperature of approximately 10 mK'.**
- **In the last paragraph, the authors mention in-situ calibration as a capability of their setup, and it is strongly implied that the data presented are calibrated. However, it is never explicitly stated whether the data shown are indeed calibrated. We suggest clarifying this point. Additionally, it would be helpful to specify that the applied calibration is a scalar calibration of the transmission parameters only, as a complete set of calibration standards (e.g., SOLR, TRL, etc.) hasn't been used.**

Results – Summary of the fabricated batches

- **In the second and third paragraphs, the authors provided information about changes in fabrication parameters, such as pressure and UV wavelength. It would be helpful to include these parameters in Table 2, so that readers can more easily make comparisons and draw their own conclusions.**
- **Could you provide a more detailed discussion on how the resistivity of the transmission line is estimated? Since the four-terminal measurement yields a value for the normal-state resistance, what method do you use to extract the resistivity, given that the conductor has a non-uniform structure (fishbone structure)?**
- **In the fourth paragraph the term "envelope" might generate confusion - we assumed it refers to the ensemble of the grey curves. In our opinion, a term such as 'overlay' would be clearer and more appropriate in this context.**
- **Figure 4: To improve the visibility of the experimentally measured band gaps (orange curves), we suggest plotting them on top of the blue curves rather than underneath.**
- **In the fifth paragraph, the authors refer to a superconducting gap voltage of 1.33 mV for the TiN film. Could the authors clarify the origin of this specific value for the initial simulations and, if possible, provide a reference to support it?**
- **For completeness, we suggest including a clear definition of the surface resistance Rs.**

Results – Device characterisation

- **Figure 5: The caption refers to a linear fitting model that does not match the description provided in the main text. We suggest ensuring consistency between the figure caption and the text.**
- **While discussing the data presented in Figure 6, the authors refer to a 'lossy non-linear regime'. Although the nonlinearity is evident from the power-dependent response, the rationale behind characterizing this regime as 'lossy' remains unclear. In particular, Figure 6b appears to display features consistent with a resonance bifurcation. We would like to draw the authors' attention to a recent study (https://iopscience.iop.org/article/10.1088/1361-6668/aca4a6), which offers an analytical treatment of nonlinear distortions in TiN resonators. This work demonstrates that distortions similar to those observed in Figure 6(b) can arise without any reduction in the internal quality factor, suggesting that the nonlinear**

behaviour is primarily reactive rather than dissipative. While the experimental conditions may not be identical, this casts some doubt on the appropriateness of the term 'lossy' in this context. We encourage the authors to reconsider their interpretation of the data in light of these findings, and, if necessary, revise the terminology used.

- **The acronym DP-4WM is not properly introduced.**
- **Regarding Figure 7, the main text states that the authors are plotting the 'change in transmission', whereas the figure caption refers more generically to 'transmission'. If the data shown represent a quantity analogous to ΔS21, we suggest updating the axis label and the caption accordingly to avoid confusion. Conversely, if the curves correspond to the actual transmission profiles under pumping, it would be helpful to also include the unpumped transmission on the same graph, as this would more clearly highlight the effect of the pump.**
- **While discussing the results presented in Figure 9, the authors attribute the power-dependent losses to an increase in quasiparticle population in the medium. In addition to this explanation, we suggest considering that the pump tone itself may alter the dispersion relation of the KITWPA by modifying the kinetic inductance of the film. This change could lead to an increased impedance mismatch along the line, which may also contribute to the observed losses. We recommend including this additional consideration in the discussion and throughout the rest of the text, as it may offer a more complete interpretation of the experimental observations.**
- **Figure 9 caption: The notation 'S21' is missing proper subscript formatting.**

Results – DC-3WM measurements

- **We do not fully agree with the authors' statement that 'Figure 8 clearly shows that the wave mixing processes are taking place.' If this were the case, one would expect to observe regions in the S21 spectrum showing a positive change in transmission, as a result of energy transfer from the pump tone to the signal tone. What is evident instead is that, at higher pump frequencies, forward transmission improves. However, this could also be explained by a better impedance matching condition, influenced by the presence and characteristics of the pump tone, rather than by the onset of mixing processes. We therefore recommend that the authors revise their interpretation of the results in Figure 8 with a more cautious perspective.**
- **The authors are encouraged to clarify in the text whether the gain reported in Figure 10 refers to an absolute gain, obtained through scalar calibration of the scattering parameter, or rather to a relative pump-on/pump-off gain.**

Conclusions

- **The statement regarding the thickness of 'other devices reported in the literature' lacks citation. Please include one or more references to substantiate this point.**

Is the work clearly and accurately presented and does it cite the current literature?
Partly

Is the study design appropriate and does the work have academic merit?
Yes

Are sufficient details of methods and analysis provided to allow replication by others?

Yes

If applicable, is the statistical analysis and its interpretation appropriate?
Partly

Are all the source data underlying the results available to ensure full reproducibility?
Yes

Are the conclusions drawn adequately supported by the results?
Partly

Competing Interests: No competing interests were disclosed.

Reviewer Expertise: Modeling, Design, Fabrication, and Characterization of Josephson Traveling-Wave Parametric Amplifiers

We confirm that we have read this submission and believe that we have an appropriate level of expertise to confirm that it is of an acceptable scientific standard, however we have significant reservations, as outlined above.

Reviewer Report 14 May 2025

https://doi.org/10.21956/openreseurope.21510.r53463

© 2025 Howe L. This is an open access peer review report distributed under the terms of the Creative Commons Attribution License, which permits unrestricted use, distribution, and reproduction in any medium, provided the original work is properly cited.



Logan Howe
NIST; University of Colorado, Boulder), Boulder, Colorado, USA

The authors present an initial attempt at demonstrating a kinetic inductance traveling wave parametric amplifier (KITWPA) using titanium nitride (TiN) as the high kinetic inductance material. The motivation provided for exploring TiN, compared to the much more common niobium titanium nitride (NbTiN), provided lies in statements regarding its mechanical strength, and both lower and tunable superconducting transition temperature. While sufficient nonlinearity was achieved to demonstrate nominal frequency shifts in test resonators and a small amount of gain in a KITWPA (<5 dB) the authors struggled to make functional devices and, in my opinion, to understand why their devices were not behaving as expected. This is confounded by the fact that the KITWPA design was more complex than necessary – featuring multiple engineered dispersion features – making understanding the complicated experimental results that much more difficult. There is also a general lack of sufficient detail in the device modeling and misinterpretation of experimental results. I believe the authors are on-track for a high quality demonstration but substantial progress understanding their fabricated TiN film and devices is necessary. In its current form I cannot recommend indexing of this manuscript.
General comments:

- The authors make a number of decisions to adjust physical parameters to make the data fit

their model without providing proper supporting measurement or analysis. Chiefly, these are the tuning of the superconducting gap voltage and assertion that their TiN film displays lower loss than expected by BCS theory. While the former is an acceptable and even expected adjustment when fine tuning a fabrication process, i.e. dirty superconductors coming out of clean rooms routinely do not display the ideal BCS-calculated gap energy, no measurements demonstrating a lower-than-expected superconducting transition temperature are provided. The latter assertion, that new physics is somehow at play and responsible for decreasing the loss in their films, is not appropriate without significantly more discussion, modeling and modeling details, simple experimental test structures and measurements, and supporting theory. Some examples of useful measurements that would help are:
    - Film critical temperature measurement.
    - Dielectric loss measurement per unit length of a length of CPW known to be defect-free.
    - Critical current of a defect-free device.
    - Internal quality factor calculation of the test resonator considering the appropriate coupling Q.
- Insufficient references are provided regarding other literature regarding both KITWPAs using NbTiN, as well as other kinetic inductance materials applications from groups other than JPL – e.g. NIST, SRON, etc.
- The S21 vs S12 asymmetry measurements are not correctly interpreted. Please see the annotated pdf for my discussion on this matter.
- The assertion that Copper pair breaking from a multi-pump-photon process is tenuous. This would have to be a very high order interaction, in which case it would be strongly suppressed. More likely there is either localized heating from dielectric loss or weak links due to defects in the centerline – especially since the authors are clear that this is common and expected in their devices.
- Extraction of the scaling current is not rigorously correct. Please see the corresponding comment in the annotated pdf. Essentially all that is needed on top of the measurement provided is a time domain reflectometry measurement of the device's full electrical length at zero dc bias.

Is the work clearly and accurately presented and does it cite the current literature?
No

Is the study design appropriate and does the work have academic merit?
Partly

Are sufficient details of methods and analysis provided to allow replication by others?
No

If applicable, is the statistical analysis and its interpretation appropriate?
Not applicable

Are all the source data underlying the results available to ensure full reproducibility?
Yes

Are the conclusions drawn adequately supported by the results?
No

Competing Interests: No competing interests were disclosed.

Reviewer Expertise: Superconducting devices, kinetic inductance traveling wave parametric amplifiers, quantum information science, detector physics.

I confirm that I have read this submission and believe that I have an appropriate level of expertise to state that I do not consider it to be of an acceptable scientific standard, for reasons outlined above.